Discrete Analogs Applied to Homogenization

Wouter Zijl
Netherlands Institute of Applied Geoscience TNO,
P.O. Box 80012, NL-3508 TA Utrecht, The Netherlands
E-mail: w.zijl@nitg.tno.nl

ABSTRACT: The coupling of software for visualization and/or pattern recognition with software for process modeling may be considered as one of the most challenging tasks for the future. Many visualization packages are based on tetrahedral meshes. In principle, such meshes offer also a good basis for numerical process modeling, like simulation of porous media flow and geomechanic phenomena. For porous media flow we have developed our own finite element software with upper and lower bound modules to assess error bounds. Numerical examples related to homogenization will exemplify the theory.

KEYWORDS: complementarity, finite elements, geomechanics, homogenization, porous media flow, simplicial cell-complexes, tetrahedral meshes

1. INTRODUCTION

The coupling of software for visualization and/or pattern recognition with software for process modeling may be considered as one of the most challenging tasks. Many visualization packages are based on tetrahedral cell-complexes (Paoluzzi et al., 1993). In principle, tetrahedral complexes offer also a good basis for numerical simulation of porous media flow and geomechanic phenomena, especially when grid refinements are important. One of the complications of such a coupling is the difference in scale between the resolution of visualization tools and that of process modeling software. To handle this mismatch, we have developed numerical methods to homogenize the process parameters absolute and relative permeability, capillary pressure, rigidity and creep viscosity. For the numerical homogenization of porous media we have developed our own finite element software. Both upper and lower bound methods have been developed to assess a posteriori error bounds. Since the software is based on tetrahedral cell-complexes upon which discrete analogs of the flow equations are solved, we may see the numerical homogenization from a broader perspective, namely as an exemplification of the more general problem of coupling visualization software with process simulation software.

We present an outline of finite element methods borrowing from ideas originally developed in computational electromagnetism [Bossavit, 1998]. Since this line of thought is very appealing and adequate for our purpose, we consider it worthwhile to introduce it in the geosciences. As ‘first principles’ we consider two equations: the ‘div-side’ equation for the scalar potential (pressure, piezometric head) and the ‘curl-side’ equation for the vector potential (stream function). This way it is possible to locate Nawalany’s ‘velocity oriented approach’ [Nawalany, 1986; Zijl and Nawalany, 1993] in the context of mainstream finite elements. It will turn out that all finite element methods based on the curl-side equation are ‘velocity oriented’, thus countering the most important argument for choosing finite difference models (Modflow, Eclipse) instead of finite element models. The classical conformal-nodal finite element method (CN-FEM) for the scalar potential in porous media flow is well known [Strang and Fix, 1973]; the node-based method for the displacement is its analog in geomechanics [Zienkewicz and Taylor, 1967]. Such methods are upper bound methods; they over-estimate the homogenized mobility (in porous media flow), rigidity (in elasticity) or viscosity (in creep flow). The mixed-hybrid finite element method (MH-FEM) is less popular, but belongs nevertheless to the standard methods nowadays [Brezzi and Fortin, 1991; Chavent and Jaffré, 1986; Kaasschieter and Huijben, 1992; Raviart and Thomas, 1977; Trykozko et al., 2001; Weiser and Wheeler, 1988]. One of its most important features is its lower bound property. Supposing that CN-FEM is well known, MH-FEM will be introduced here in a more ‘physical’ way than in the standard literature, by basing it on the relatively new

edge element method for the vector potential. Bilateral error bounds have been described by Trykozko, Zijl and Bossavit [2001].

2. CELL COMPLEXES AND THEIR PROPERTIES

Topology is concerned with properties that endure when geometrical figures are transformed continuously. Metrical properties like distances between points may change, but the number of points and their relative orientations may not. As an illustration, let us consider 4D space-time. It is known from the theory of general relativity that its metric is dependent on the presence of matter. However, it is still an open question whether its topology is matter-dependent too. As Goedel has pointed out and has been affirmed by Einstein, a matter-dependent topology allows one to travel into temporal regions of the universe that have already been passed. In this paper we adopt Whitehead's topological priority above matter and accept that the universe's events cannot be repeated [Tanaka, 1985]. As a consequence, we accept 'the arrow of time' $t > 0$ in handling time-dependent process equations.

A cell is one of the simplest topological objects; it is any figure that is topologically equivalent to a ball. The topological properties of the ball are: (i) it is one piece (any attempt to divide the ball into more than one piece would require cutting, and that is forbidden in continuous transformations), and (ii) it neither loops (i.e., it is not torus-like) nor holes (i.e., it has one boundary) [Henle, 1979]. Here we will consider cells that may be glued and pasted together along their faces. This way we form simplicial cell-complexes (in 3D simplices are points, straight lines, flat faces and volumes). In principle, the simplicial cell-complex may be built up by any regular polyhedron, but we limit our discussion to tetrahedral cell-complexes, since they are used in many visualization packages and form a the simplest possible mesh in finite element methods. However, the cube is important too, since it forms the 'grid-blocks' in the popular control volume finite difference method.

Let us first, as an example, consider a cell-complex set up as a division of the modeling domain into N cubes that are divided into five tetrahedrons. The modeling domain is assumed to a cube too, so it is possible to assume periodicity: i.e., we count equivalent nodes on two opposite boundaries only once. Then there are N 'active nodes' and $T = 5N$ tetrahedrons. Since there are four faces for each tetrahedron, shared by two, there are $F = 10N$ active faces (triangles). Finally, from the Euler-Poincaré formula $N - E + F - T = \chi$, where $\chi = 1$ for simply connected domains [Weintraub, 1977], it follows that there are $E = 6N - 1$ active edges [Henle, 1979; Bossavit, 1998]. In a similar way, we can derive that a division of the cubes into six tetrahedrons leads to $T = 6N$, $F = 12N$ and $E = 7N - 1$. Looking at these numbers, the first thought that jumps to the mind is that numerical models that based on nodes as degrees of freedom (i.e., CN-FEM) perform cheapest with respect to computer time and memory. The second-cheapest methods are based on edges, while the most expensive methods are based on faces (i.e., MH-FEM). Other factors also influence the numerical efficiency, but this tendency holds. Of course, tetrahedral cell-complexes may have a much more general and 'irregular' character. For instance, they may be obtained from alpha complexes, which have originally been developed for visualization and pattern recognition [Gerritsen et al., 2001a, 2001b].

In our novel approach to process modeling, *incidence* and *orientation* are very important notions. Each edge has a 'forward direction', each face has a notion of 'turning clockwise', each tetrahedron has its own 'corkscrew rule', and even nodes are oriented, which consists in attributing a sign, + or –, to each of them (Paoluzzi, 1993). We assign to two simplices σ and s of respectively dimensions d and $d+1$ an incidence number: ± 1 if σ is a face of s and 0 otherwise. The sign, + or –, depends on whether orientations match or not. Collecting the incidence numbers in arrays, we obtain three matrices: (i) the $T \times F$ matrix D, (ii) the $F \times E$ matrix R and (iii) the $E \times N$ matrix G [Henle, 1979; Bossavit, 1998]. These incidence matrices have a very appealing meaning: D, R, G are the discrete counterparts of the spatial differential operators div, rot, grad upon which the process models are based. Indeed, for topological 'balls' $\mathrm{D}\,\mathrm{R} \equiv 0$ and $\mathrm{R}\,\mathrm{G} \equiv 0$, which are the discrete analogs of the

well-known relations $\mathrm{div}(\mathrm{rot}.) \equiv 0$ and $\mathrm{rot}(\mathrm{grad}.) \equiv \underline{0}$. However, in contrast to the partial differential operators, the incidence matrices are metric-free, they depend only on the topology of the cell-complex, which is a major advantage regarding our assumed topological priority over matter.

Finally, in process modeling, *duality* of meshes plays an important role. For a tetrahedral primal mesh, the dual mesh dual is such that that the barycenters of the tetrahedrons of the primal mesh correspond with the nodes of the dual mesh, while the faces (triangles) of the primal mesh correspond with the edges of the dual mesh, and so on. More specifically, a dual edge $\breve{e}$ belonging to primal face f is the union of the two line segments that join the barycenter of that face with the two barycenters of the tetrahedrons flanking that face. To be sure, the dual mesh is not a simplicial mesh, since the edges are *broken* lines (Fig. 4.5 from Bossavit, 1998).

3. PARADIGMATIC EQUATIONS

We exemplify our line of thought using the following equations as paradigmatic 'first principles'

$$\mathrm{div}(\underline{\underline{\lambda}} \bullet \mathrm{grad}\, \varphi) = 0 \ \text{ in } C\,. \tag{1}$$

$$\mathrm{rot}(\underline{\underline{\lambda}}^{-1} \bullet \mathrm{rot}\, \underline{a}) = \underline{0} \ \text{ in } C\,. \tag{2}$$

Both (1) and (2) describe steady single-phase fluid flow in a domain C filled with porous material. 'Div-side' equation (1) is well known in groundwater hydrology and petroleum reservoir engineering. Although 'curl-side' equation (2) is well known in the theory of electromagnetism (Maxwell presented his famous equations using a vector potential [Bossavit, 1998]), this equation is hardly known in the context of porous media flow. It is our strong conviction that (2) is extremely useful. Therefore we will focus on (2), while supposing that (1) and its discrete analogs are well known. Here $\underline{\underline{\lambda}}$ $\{\mathrm{m}^2.\mathrm{Pa}^{-1}.\mathrm{s}^{-1}\}$ is the mobility tensor (the intrinsic permeability divided by the viscosity), φ $\{\mathrm{Pa}\}$ is the (scalar) potential, and $\underline{a}$ $\{\mathrm{m}^2.\mathrm{s}^{-1}\}$ is the vector potential.

The (scalar) potential is the fluid pressure minus the hydrostatic pressure. Consider groundwater with a density of $1000\ \mathrm{kg.m}^{-3}$ in a gravitational field of $10\ \mathrm{m.s}^{-2}$, then a piezometric height of $1\ \mathrm{m}$ corresponds with a water pressure of $1\ \mathrm{dbar} = 10{,}000\ \mathrm{Pa}$. In other words, we may equate the numerical value of the piezometric head to that of the potential expressed in decibar. Similarly, we may equate the mobility to the hydraulic conductivity. However, for oil, which has a different density, this 'trick' is no longer allowed.

In contrast to what is generally believed, the vector potential has a physical meaning too. In a plane normal to the its direction, its absolute value times a metric coefficient is the stream function. However, we will not go deeper into this interpretations here. The flux density $\{\mathrm{m.s}^{-1}\}$ (the specific discharge) is given by $\underline{q} = \mathrm{rot}\, \underline{a} = -\underline{\underline{\lambda}} \bullet \mathrm{grad}\, \varphi$.

Equations (1) and (2) can easily be extended to steady multi-phase flow. In the numerical examples we focus on two-phase flow [Zijl and Trykozko, 2001b]. Extensions to elastic geomechanics and creep of viscous rock layers are possible too.

Although (1) and (2) are mathematically equivalent, their discrete analogs are not. This gives rise to two different numerical approximation methods, which can be used to establish error bounds. Numerical examples of the error bounds will be presented below, while for the theory reference is made to Trykozko, Zijl and Bossavit [2001].

4. DISCRETE ANALOGS OF THE PARADIGMATIC EQUATIONS

4.1. The curl side

We assign to each face f of the tetrahedral primal mesh a flux $q_f = \iint_f \underline{q} \bullet \underline{\nu}_f dS$ $\{\mathrm{m}^3.\mathrm{day}^{-1}\}$ through that face. Let us denote by q the array of face-based fluxes and consider the following linear system

$$\mathrm{D}\,\mathrm{q} = 0 . \tag{3}$$

System (3) is equivalent with $\sum_f q_f = 0$, where the summation is over the four faces of a tetrahedron. Hence (3) expresses mass conservation for each tetrahedron.

We assign a potential difference $h_f = \int_{\breve{e}} \underline{h} \bullet \underline{\tau}_{\breve{e}}\, d\breve{\ell}$ $\{\mathrm{dbar}\}$ along each dual edge $\breve{e}$. Let h be the column array of face-based potential differences, then the system

$$\mathrm{R}^T\,\mathrm{h} = 0 \tag{4}$$

is equivalent with $\sum_{\breve{e}} h_f = 0$, which means that the circulation of $\underline{h}$ is zero along the edges of a dual face, from which it follows that $\underline{h} = -\mathrm{grad}\,\varphi$ along the edges of each dual face.

Equations (3) and (4) are metric-free; only the topology of the mesh matters. The metric comes in by the discrete analog of Darcy's law

$$\mathrm{q} = \mathrm{L}\,\mathrm{h} . \tag{5}$$

The square $F \times F$ matrix L $\{\mathrm{m}^3.\mathrm{Pa}^{-1}.\mathrm{s}^{-1}\}$ may be constructed by a control volume finite difference approach [Bossavit, 1999], but in the context of finite elements L is obtained by the Galerkin approach [Bossavit, 1998]

$$[\mathrm{L}^{-1}]_{ij} = \iiint_C \underline{w}_i \bullet \underline{\underline{\lambda}}^{-1} \bullet \underline{w}_j dV , \tag{6}$$

where the mobility $\underline{\underline{\lambda}}$ is tetrahedron-wise constant. The vector function $\underline{w}_f$ is defined as

$$\underline{w}_f = 2(w_\ell \mathrm{grad}\, w_m \times \mathrm{grad}\, w_n + w_m \mathrm{grad}\, w_n \times \mathrm{grad}\, w_\ell + w_n \mathrm{grad}\, w_\ell \times \mathrm{grad}\, w_m) , \tag{7}$$

where face f is oriented from node ℓ via node m to node n. Scalar function w_n is the well-known continuous piecewise linear 'hat' function that is equal to 1 at node n and 0 at other nodes. Since the mobility $\underline{\underline{\lambda}}$ is a symmetric and strictly positive definite tensor, the matrix L is also symmetric and strictly positive definite.

Combination of (4) and (5) using (6) leads to the algebraic system

$$\mathrm{R}^T\,\mathrm{L}^{-1}\,\mathrm{q} = 0 . \tag{8}$$

To transform the above system to a solvable $E \times E$ system, the relation $\mathrm{D}\,\mathrm{R} \equiv 0$ is invoked. Writing this relation written as $\mathrm{D}\,(\mathrm{R}\,\mathrm{a}) \equiv 0$, and recalling that $\mathrm{D}\,\mathrm{q} \equiv 0$, suggests to introduce an array a of edge-based degrees of freedom a_e such that $\mathrm{q} = \mathrm{R}\,\mathrm{a}$. Indeed, this way we obtain the discrete analog of $\underline{q} = \mathrm{rot}\,\underline{a}$. Here $a_e = \int_e \underline{a} \bullet \underline{\tau}_e\, d\ell$ $\{\mathrm{m}^3.\mathrm{day}^{-1}\}$ is the tangential component of the vector potential integrated over primal edge e. Moreover, $q_f = \sum_e a_e$, i.e., the circulation of $\underline{a} \bullet \underline{\tau}$ along the edges of a primal face is equal to the flux through that face. This finally leads to the algebraic system

$$\mathrm{R}^T\,\mathrm{L}^{-1}\,\mathrm{R}\,\mathrm{a} = 0 , \tag{9}$$

of which the $E \times E$ matrix $\mathrm{R}^T\,\mathrm{L}^{-1}\,\mathrm{R}$ is sparse and symmetric. System (9) is the discrete analog of (2).

Since in (1) and (9) there is no requirement for $\mathrm{div}\,\underline{a}$, physical boundary conditions can easily be inserted [Bossavit, 1998]. The resulting system has a positive semi-definite matrix with null space containing the range of G (i.e., the solution $\underline{a}$ is unique up to an arbitrary function $\mathrm{grad}\,f$). This system can be solved by a conventional preconditioned conjugate gradient method [Bossavit, 1998; Kaasschieter, 1988; Meijerink and Van der Vorst, 1977].

4.2. The div side

Using a similar line of thought, the discrete analog of (1) yields the system of equations

$$\mathrm{G}^T\ \mathrm{L}^*\ \mathrm{G}\,\mathrm{p}^* = 0\,, \tag{10}$$

where p^* is the array of node-based scalar potentials and $[\mathrm{L}^*]_{ij} = \iiint_C \underline{w}_i \bullet \underline{\underline{\lambda}} \bullet \underline{w}_j dV$, $\underline{w}_e = w_m \mathrm{grad}\, w_n - w_n \mathrm{grad}\, w_m$, is the well-known $N \times N$ system matrix that belongs to the 'classical' conformal-nodal finite element method (CN-FEM) [Strang and Fix, 1997; Zienkewicz and Taylor, 1967]. Note that G^T is the discrete analog of the divergence in the dual mesh. In other words, system (10) is equivalent with $\sum_{\breve{f}} q_{\breve{f}} = 0$; the summation is over the faces $\breve{f}$ of a dual volume. Hence (10) expresses mass conservation for each dual volume (Figure 4.5 from Bossavit, 1998).

Systems (9) and (10) are complementary in the sense that system (9) gives lower bounds for the eigenvalues of the numerically approximated coarse-scale mobility, while system (10) gives upper bounds [Trykozko, Zijl and Bossavit, 2001].

5. DISCRETE FLUX-BASED PROCESS MODELS

Edge elements for the vector potential are used in computational electromagnetics, because in that branch of science the vector potential is generally accepted as a quantity with 'physical meaning'. However, when considering computational porous media flow (as well as computational geomechanics), the flux densities (the tractions in geomechanics) are considered as the standard alternative to the 'classical' potentials (pressures, piezometric heads). Moreover, node elements have a long history and are, therefore, well established. Edge elements are relatively new and have not (yet) penetrated into the earth sciences. Therefore, it has been considered in the past as worth while to develop node-based methods for the flux density.

The simplest idea that jumps to the mind is to derive 'div-side' equations for the flux density. Taking the curl of (2) and using the relation $\mathrm{rot}(\mathrm{rot}\,.) = \mathrm{grad}(\mathrm{div}\,.) - \mathrm{div}(\mathrm{grad}\,.)$ yields $\mathrm{div}(\lambda^{-1}\ \mathrm{grad}\ q_i) + \mathrm{div}(q_i\ \mathrm{grad}\ \lambda^{-1}) - \partial_i(\underline{q} \bullet \mathrm{grad}\ \lambda^{-1}) = 0$ for any *isotropic* medium. If we assume perfect layering, e.g., $\lambda = \lambda(z)$, we find an equation for q_z that has the same baffling simplicity as (1)

$$\mathrm{div}(\lambda^{-1}\mathrm{grad}\ q_z) = 0 \ \text{ in } C\,. \tag{11a}$$

Again assuming that the medium is *perfectly layered*, taking the x and y derivative of (1) yields

$$\mathrm{div}(\lambda\ \mathrm{grad}\ h_x) = 0\,,\ \mathrm{div}(\lambda\ \mathrm{grad}\ h_y) = 0 \ \text{ in } C\,, \tag{11b,c}$$

Equations (11b,c) are a special case of div-side equation (1), while (11a) is a special case of curl-side equation (2) in div-side disguise. The numerical solution of these equations leads automatically to complementary algebraic systems and, hence, to a posteriori error bounds. Instead of solving the relatively complicated equations (1), (2), the much simpler task of solving their equivalents (11) by well established node-based finite elements has been accomplished by Nawalany [1986], who obtained extremely accurate solutions using the software he developed. In addition, (11) has formed the basis of practical engineering results regarding the calculation of vertical flux densities from solutions to the Dupuit approximation in aquifers, as well as regarding the upscaling to aquifer transmissivities [Zijl and Nawalany, 1993]. Despite these successes, we have to consider the 'mother equations' (1), (2) if we are interested in more general mobility patterns.

The mixed-hybrid finite element method (MH-FEM) is an alternative curl-side method that is not based on the vector potential. Using the identity $\mathrm{R}^T\mathrm{D}^T \equiv 0$ – the discrete analog of $\mathrm{rot}(\mathrm{grad}\,.) \equiv 0$ in the dual mesh – (4) yields

$$\mathrm{h} = \mathrm{D}^T\ \mathrm{p}\,, \tag{12}$$

where p is the array of discrete scalar potentials p_t at the dual nodes (the barycenters of the tetrahedrons). This way, equations (3) and (5) yield the mixed system [Trykozko, Zijl and Bossavit, 2001]

$$\begin{pmatrix} \mathrm{L}^{-1} & \mathrm{D}^T \\ \mathrm{D} & 0 \end{pmatrix} \bullet \begin{pmatrix} \mathrm{q} \\ \mathrm{p} \end{pmatrix} = \begin{pmatrix} 0 \\ 0 \end{pmatrix} \tag{13}$$

Left multiplying the upper equations of (13) by R^T and using (4) and (12) yields (8) and, hence, (9). Moreover, since the null space of R^T is the range of D^T, the inverse procedure, starting with (8) and ending up with (13), is possible too. Hence, the two systems (9) and (13) are algebraically equivalent. Since it is relatively simple to prove the convergence of (9), the algebraic equivalence is a much simpler proof of convergence of the mixed (and mixed-hybrid, see below) method than presented in the literature [Bossavit, 1998].

Since mixed system (13) has poor algebraic properties, the now classical move to the mixed-hybrid approach has been applied. Hybridization of (13) has been described extensively in the literature [Chavent and Jaffré, 1986; Kaasschieter and Huijben, 1992; Raviart and Thomas, 1977; Trykozko et al., 2001; Weiser and Wheeler, 1988]. The procedure is only briefly summarized here. First we *double* q and h such that there are two distinct values on the sides of each face. This leads to a *redefinition* of q, h, L, D, R, etc., denoted here as q', h', L', D', R'. This step may be considered as a domain decomposition technique for each tetrahedron. Now the constraint $\mathrm{M}\,\mathrm{q}' = 0$ expresses the continuity of normal fluxes on all faces, where matrix M has a very simple structure. The constraints are introduced using a face-based Lagrange multiplier array ℓ. The Lagrange multiplier of each face represents the potential difference between the two adjacent dual nodes. Although the meaning of q', h', etc., has changed, this yields a new, but algebraically equivalent version of (9) and (13)

$$\begin{pmatrix} -\mathrm{L}'^{-1} & \mathrm{D}'^T & \mathrm{M}^T \\ \mathrm{D}' & 0 & 0 \\ \mathrm{M} & 0 & 0 \end{pmatrix} \bullet \begin{pmatrix} \mathrm{q}' \\ \mathrm{p} \\ \ell \end{pmatrix} = \begin{pmatrix} 0 \\ 0 \\ 0 \end{pmatrix}. \tag{14}$$

Since L' is block-diagonal, q' can easily be eliminated. This way we end up with a symmetric system in terms of p and ℓ. Eliminating p we finally find an $F \times F$ system in terms of only ℓ

$$\mathrm{M}\,[\mathrm{L}' - \mathrm{L}'\mathrm{D}'^T\,\Lambda^{-1}\,\mathrm{D}'\mathrm{L}']\,\mathrm{M}^T \ell = 0, \tag{15}$$

where $\Lambda = \mathrm{D}'\,\mathrm{L}'\,\mathrm{D}'^T$ [Kaasschieter and Huijben, 1992, Trykozko et al., 2001]. System (15) may be considered as a preconditioned version of the algebraically equivalent systems (9), (13) and (14). If mobility tensor $\underline{\underline{\lambda}}$ is diagonal, the matrix Λ is also diagonal. This observation has lead to the famous proof that block-centered finite differences are nothing but a special case of mixed-hybrid finite elements [Weiser and Wheeler, 1988].

6. NUMERICAL EXAMPLE: HOMOGENISATION OF FLOW PARAMETERS

Let us consider an isotropic porous medium with absolute permeability $k(\underline{x}) = \zeta(\underline{x}) \times 10^{-3}$ $\mu\mathrm{m}^2$ ($1\,\mu\mathrm{m}^2 = 1013.250$ mD), where $\zeta(x,y,z) = 8\mu^{-1}\alpha\beta\gamma\,\cosh^2 x \cos^2 y \cosh^2 z$ in the domain $|x| \le \alpha$, $|y| \le \beta$, $|z| \le \gamma$. Outside this domain the function $\zeta(\underline{x})$ is continued periodically. The factor $\mu = (\alpha + \frac{1}{2}\sinh 2\alpha)\ (\beta + \frac{1}{2}\sin 2\beta)\ (\gamma + \frac{1}{2}\sinh 2\gamma)$ is such that $\langle\zeta\rangle = 1$ and $\langle\zeta^{-1}\rangle = 8^{-1}(\alpha\beta\gamma)^{-2}\mu \tanh\alpha \tan\beta \tanh\gamma$. In the examples we have chosen $\alpha = \gamma = 49/50$ and $\beta = 49\pi/100$.

The water has viscosity $\eta_1 = 5\times10^{-4}$ Pa.s = 0.5 cp, while the oil has viscosity $\eta_2 = 5\times10^{-2}$ Pa.s = 50 cp. The relative permeabilities are $r_1(s_1) = \frac{2}{3}(s_1^{2\zeta(\underline{x})} - (\frac{1}{10})^{2\zeta(\underline{x})})$ and $r_2(s_2) = \frac{8}{7}(s_2^{2\zeta(\underline{x})} - (\frac{1}{5})^{2\zeta(\underline{x})})$. The capillary pressure is given by $p(\underline{x}, s_1)/p_0 = b\tan((9-20s_1)\pi/14) + d(\underline{x})$ (p_0 = 1 kPa = 0.1450377 psi) where either $b = 0$ and d is constant (the no-capillary gradient case) or $b = 1$ and $d(\underline{x}) = 5\zeta(\underline{x})^{-1}/2$ (the saturation-dependent capillary case). The admissible interval for the water saturation is $1/10 \le s_1 \le 4/5$; the residual oil saturation is 1/5 and the maximum oil saturation is 9/10. In this example the exact coarse-scale absolute permeability $\underline{\underline{K}}$ is given by the diagonal matrix $\mathrm{diag}(K_{xx}, K_{yy}, K_{zz}) = \mathrm{diag}(F_x, F_y, F_z)\times10^{-3}$ $\mu m^2.Pa^{-1}.s^{-1}$, where $F_x = 2\alpha^2\coth\alpha/(\alpha + \frac{\sinh 2\alpha}{2})$, $F_y = 2\beta^2\cot\beta/(\beta + \frac{\sin 2\beta}{2})$ and $F_z = 2\gamma^2\coth\gamma/(\gamma + \frac{\sinh 2\gamma}{2})$ [Trykozko et al., 2001; Zijl and Trykozko, 2001a]. In the finite element analogs, where the fine-scale mobility is tetrahedron-wise constant, we assign to each tetrahedron the fine-scale mobility using the above expressions in its barycenter.

To perform the numerical experiments, the following nine values of ν have been specified: 0.0001, 0.0003, 0.001, 0.01, 0.1, 1, 10, 100, 300. The bisection method [Press et al., 1986] is used with termination criterion $|r_2(s_2)/r_1(s_1) - \nu| \le 10^{-8}$ yielding the coarse-scale saturations s_β for each specified ν from which the corresponding mobilities are calculated. To solve the saturation-dependent capillary case, the saturations obtained from the no-capillary-gradient case have been chosen as initial values for the successive iteration procedure. The results obtained for the saturation-dependent capillary pressure are shown in Figures 1—3. Only values obtained with CN-FEM are reported.

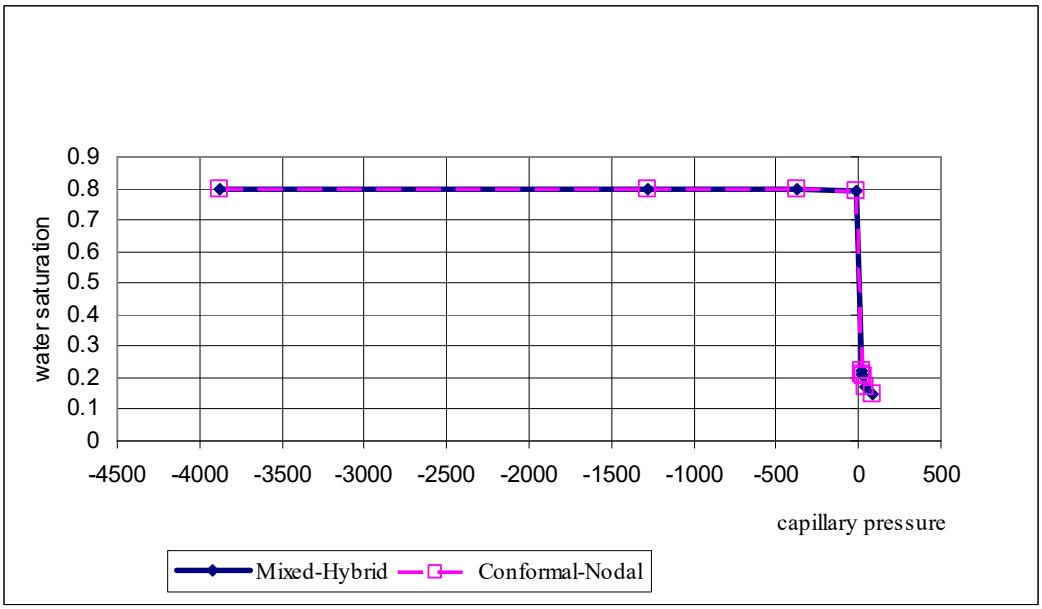

Figure 1. Coarse-scale water saturation S_1 vs. coarse-scale capillary pressure P.

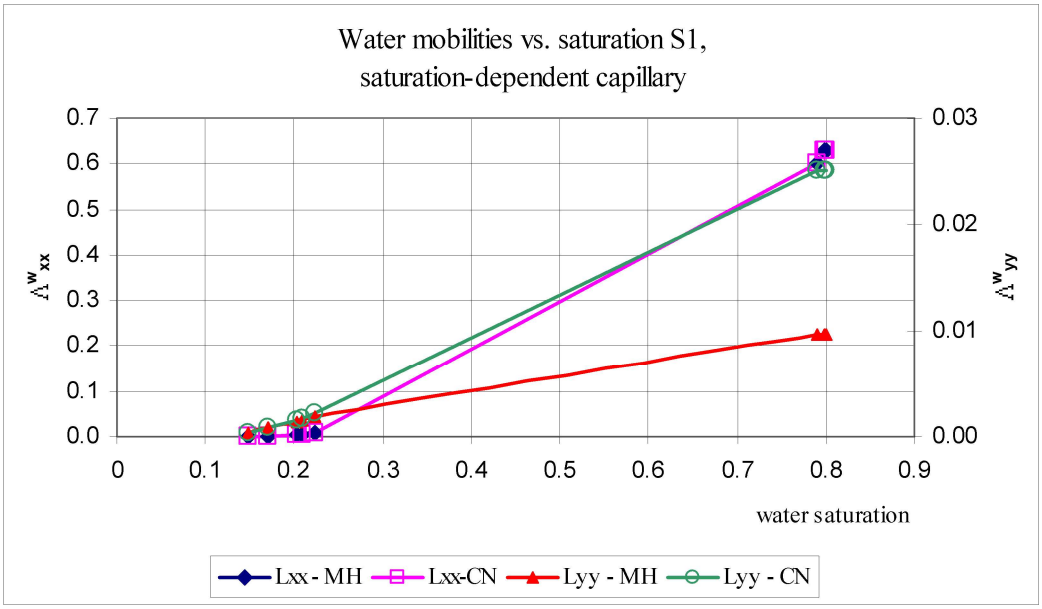

Figure 2. Coarse-scale water mobilities Λ_{ij}^{w} vs. coarse-scale water saturation S_1.

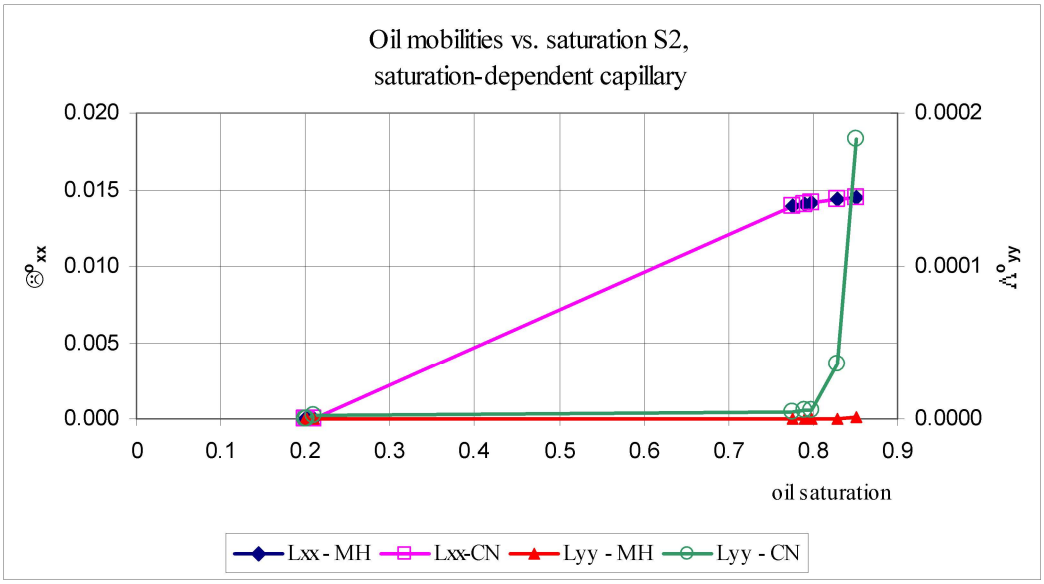

Fig. 3. Coarse-scale oil mobilities Λ_{ij}^{o} vs. coarse-scale oil saturation S_2.

Since we have access to two algebraically different approximation methods, there is a temptation to compare their behavior. Thus, a set of computational experiments has been performed aiming to study the two approximate solutions. Only the parameter value $\nu = 0.1$ has been chosen for that purpose. The computations were performed for a sequence of uniformly refined meshes. The results are summarized in Figures 4—7.

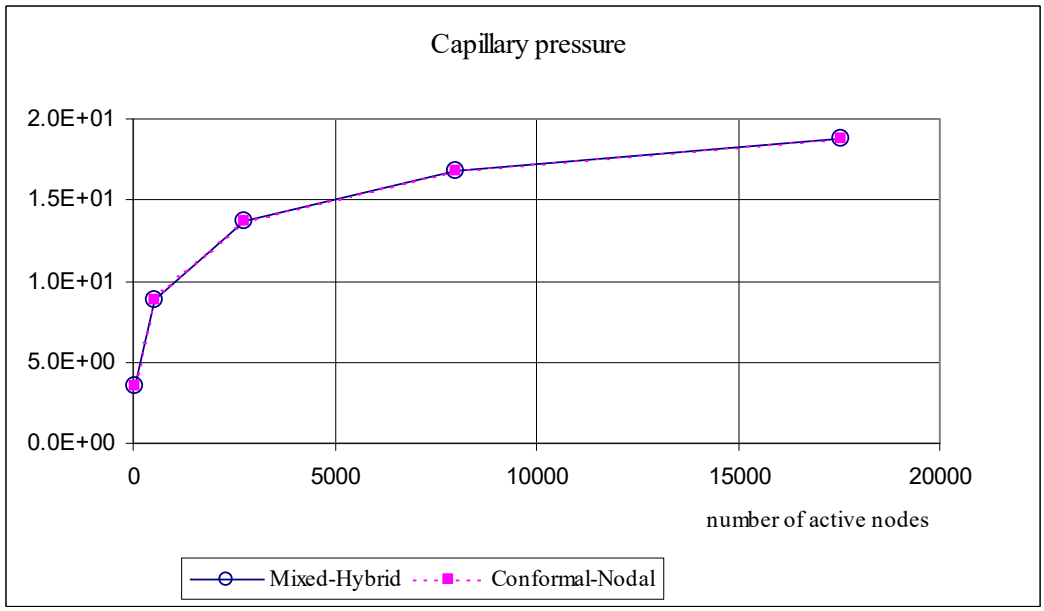

Figure 4. Coarse-scale capillary pressure vs. number of active nodes.

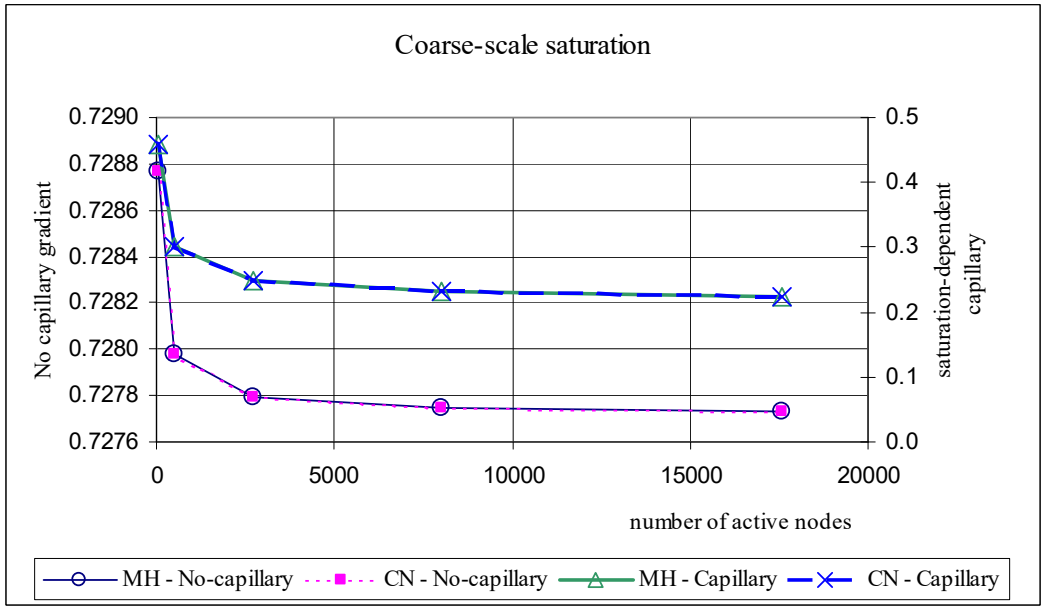

Figure 5. Coarse-scale water saturation vs. number of active nodes.

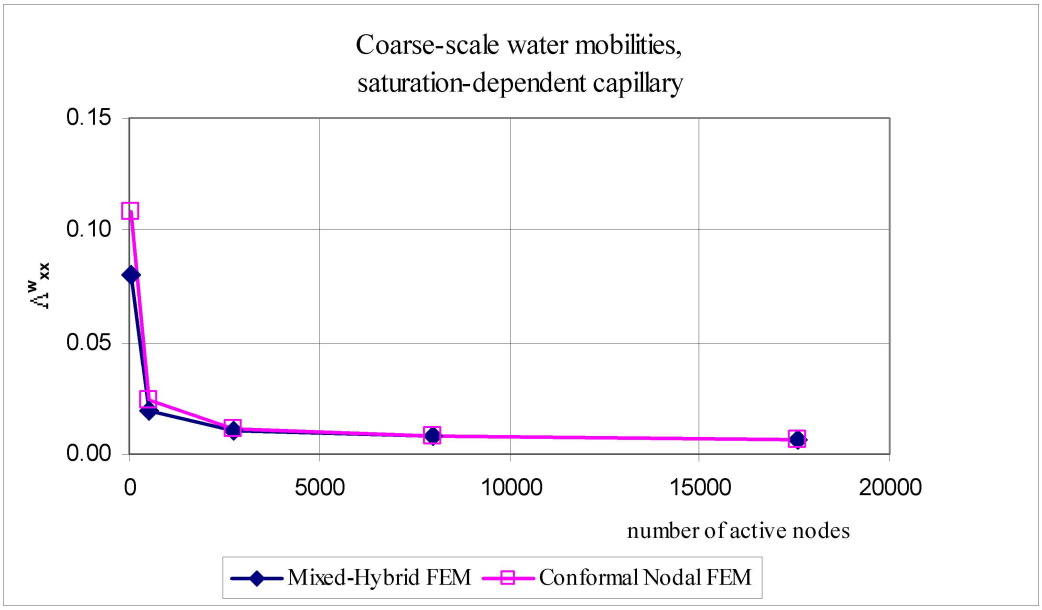

Figure 6. Saturation-dependent capillary: coarse-scale water mobilities Λ^w_{xx} vs. number of active nodes.

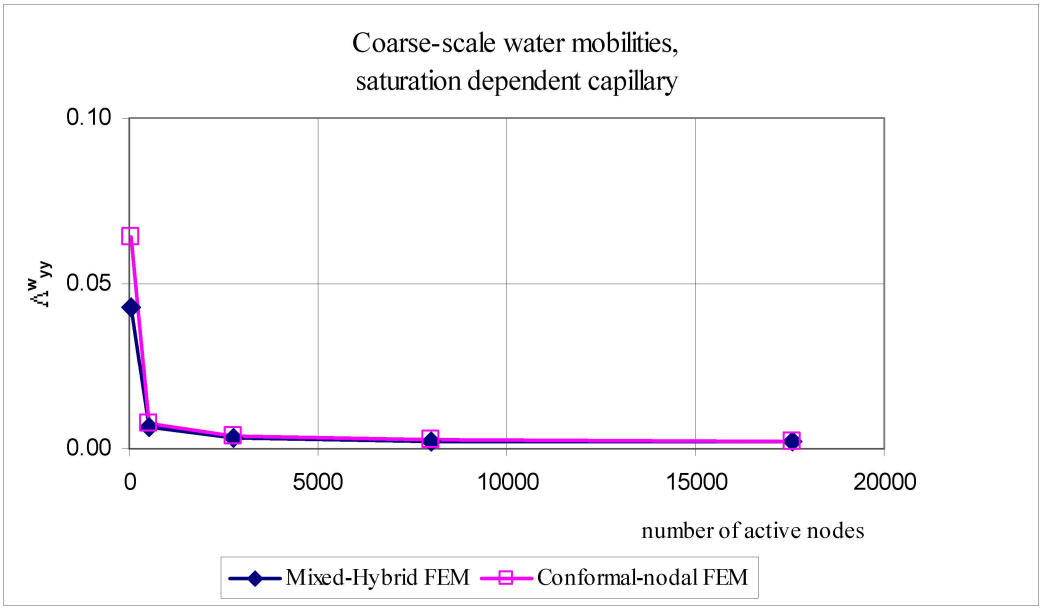

Figure 7. Saturation-dependent capillary: coarse-scale water mobilities Λ^w_{yy} vs. number of active nodes.

The two methods provide solutions that are very close to each other. In general, the differences in the *yy* component between two solutions are greater. This is due to the form of the fine-scale absolute permeability, which is steeply descending to zero near the *y*-boundaries.

The function describing the fine-scale absolute permeability is continuous, while the two finite-element methods use tetrahedron-wise constant fine-scale mobility values. Hence, for each mesh in the sequence of meshes used in the computations another discrete problem is derived from the continuous problem. For each problem in the sequence of discrete problems, the CN-FEM and MH-FEM solutions represent respectively the upper and lower bounds, although the CN-FEM and MH-FEM solutions presented do not bound the exact solution of the continuous problem.

7. SUMMARY AND CONCLUSIONS

We have shown that tetrahedral cell-complexes are not only useful for visualization and pattern recognition, but also for process modeling. The essential step from cell-complexes to process simulations is the application of the equivalence between the three incidence matrices of a cell-complex with the three spatial differential operators from process models. Considering two mathematically equivalent process equations – the 'div-side' and the 'curl-side' equation – as 'first principles', we were able to derive the well-known conformal-nodal finite element method (CN-FEM), as well as a realm of algebraically equivalent complementary finite element methods, which are not algebraically equivalent with CN-FEM. The mixed-hybrid finite element method (MH-FEM) is the most popular complementary method, but the newer edge element method seems very promising and deserves further research. Arguments are given showing that CN-FEM combined with edge elements may be considered as a generalization of Nawalany and Zijl's velocity-oriented finite elements. The div-side equations have been solved numerically to determine upper bounds, while the 'curl side' equations have been used to compute lower bounds. Homogenization of two-phase flow parameters has been chosen as a numerical example.

For future R&D we recommend to build relatively simple, hence fast, process models in the software for visualization and pattern recognition. If this latter software is based on tetrahedral cell-complexes, this can easily be accomplished using the incidence matrices and (6). To make the models fast, data reduction by numerical homogenization is proposed.

Acknowledgements

We gratefully acknowledge Alain Bossavit (Électricité de France) for his inspiring enthusiasm to base mixed-hybrid finite elements on the algebraically equivalent edge elements. We also gratefully acknowledge Bart Gerritsen (TNO-NITG) for his enthusiasm to promote topological concepts, especially alpha-complexes, in the earth sciences. Finally, we gratefully acknowledge the support of the Banach Centre of Excellence (Warsaw).

8. REFERENCES

Bossavit, A., *Computational Electromagnetism: Variational Formulations, Complementarity, Edge Elements* (Academic Press, San Diego, 1998).

Bossavit, A., Computational electromagnetism and geometry: building a finite-dimensional "Maxwell's house", J. Japan Soc. Appl. Electromagn. & Mech. 7 (1999) 150-159 (part 1), 294-301 (part 2), 401-408 (part 3).

Brezzi, F. and M. Fortin, *Mixed and Hybrid Finite Element Methods* (Springer-Verlag, New York, 1991).

Chavent, G., and J. Jaffré, *Mathematical Models and Finite Elements for Reservoir Simulation* (North Holland Publishing Comp., Amsterdam, 1986).

Gerritsen, B.H.M., K. van der Werff and R.C. Veltkamp, Modelling natural objects with alpha complexes, Computer Aided Design, Special Issue on TMCE, 2001 (accepted).

Gerritsen, B.H.M., W. Zijl, and A. Trykozko, From alpha complexes to finite element analysis: exemplified by Barchan dune avalanching, Computing and Visualization in Science, 2001 (submitted).

Henle, M., *A Combinatorial Introduction To Topology* (W.H. Freeman and Company, San Francisco, 1979).

Kaasschieter, E.F., Preconditioned conjugate gradients for solving singular systems, Journal of Computational and Applied Mathematics 24 (1988) 265-75.

Kaasschieter, E.F., and A.J.M. Huijben, Mixed-hybrid finite elements and streamline computations for the potential flow problem, Numerical Methods for Partial Differential Equations 8 (1992) 221-226.

Meijerink, J.A., and H.A. van der Vorst, An iterative solution method for linear systems of which the coefficient matrix is a symmetric M-matrix, Mathematics of Computations 31 (1977) 148-162.

Nawalany, M., FLOSA-3D, Introduction to system analysis of three-dimensional groundwater flow (TNO-NITG Report No. OS 86-07, Delft/Utrecht, 1986).

Paoluzzi, A., F. Bernardini, C. Cattani and V. Ferrucci, Dimension-independent modeling with simplicial complexes, ACM Transactions on Graphics, Vol. 12, No. 1, January 1993, pp. 56-102.

Press, W.H., S.A. Teukolsky, W.T. Vetterling and B.P. Flannery, *Numerical Recipes in FORTRAN: The Art of Scientific Computing* (Cambridge University Press, New York, 1986).

Raviart, R.A., and J.M. Thomas, A mixed finite element method for 2nd order elliptic problems, In: Mathematical Aspects of the Finite Element Method, Lecture Notes in Math. 606, Springer-Verlag, New York (1977) 292-315.

Strang, G. and G.J. Fix, An Analysis of the Finite Element Method (Prentice-Hall, Inc., Englewood Cliffs, 1973).

Tanaka, Y., The comparison between Einstein's and Whitehead's theory of relativity, 1st and 2nd Whitehead Relativity Conference, Claremont, Calif., Nov. 1984 and Oct. 1985 (www.asahi-net.or.ip/~sn2y-

tnk/tanaka_4_0.htm).
Trykozko, A., W. Zijl and A. Bossavit, Nodal and mixed finite elements for the numerical homogenization of 3D permeability, Computational Geosciences (2001) (accepted).
Weintraub, S.H., Differential Forms (Academic Press, San Diego, 1977).
Weiser, A., and M.F. Wheeler, On convergence of block-centered finite differences for elliptic problems, SIAM J. Numerical Analysis 25 (1988) 351-375.
Zienkewicz, O.C. and R.L. Taylor, *The Finite Element Method* (MacGraw-Hill, London, 1967).
Zijl, W., and M. Nawalany, *Natural Groundwater Flow* (Lewis Publishers / CRC Press, Boca Raton, 1993).
Zijl, W. and A. Trykozko, Numerical homogenization of the absolute permeability using the conformal-nodal and the mixed-hybrid finite element method, Transport in Porous Media (2001a) (in print).
Zijl, W. and A. Trykozko, Numerical homogenization based on complementary finite elements applied to nonlinear flow in porous media and viscous layers, Computational Geosciences (2001b) (submitted).